Retrieval of water-leaving radiance and aerosol optical thickness over the oceans with SeaWiFS: a preliminary algorithm

Howard R. Gordon and Menghua Wang

The second generation of ocean-color-analyzing instruments requires more accurate atmospheric correction than does the Coastal Zone Color Scanner (CZCS), if one is to utilize fully their increased radiometric sensitivity. Unlike the CZCS, the new instruments possess bands in the near infrared (NIR) that are solely for aiding atmospheric correction. We show, using aerosol models, that certain assumptions regarding the spectral behavior of the aerosol reflectance employed in the standard CZCS correction algorithm are not valid over the spectral range encompassing both the visible and the NIR. Furthermore, we show that multiple-scattering effects on the algorithm depend significantly on the aerosol model. Following these observations, we propose an algorithm that utilizes the NIR bands for atmospheric correction to the required accuracy. Examples of the dependence of the error on the aerosol model, the turbidity of the atmosphere, and surface roughness (waves) are provided. The error in the retrieved phytoplankton-pigment concentration (the principal product of ocean-color sensors) induced by errors in the atmospheric correction are shown to be $<20\%$ in approximately 90% of the cases examined. Finally, the aerosol thickness (τ_a) is estimated through a simple extension of the correction algorithm. Simulations suggest that the error in the recovered value of τ_a should be $\lesssim 10\%$.

Introduction

The Coastal Zone Color Scanner (CZCS) on Nimbus 7 was a scanning radiometer that viewed the ocean in six coregistered spectral bands, five in the visible and near infrared (443, 520, 550, 670, and 750 nm, herein labeled bands 1, 2, 3, 4, and 5, respectively) and one in the thermal infrared (10.5–12.5 μm, herein labeled band 6). The purpose of the CZCS is to provide estimates of the near-surface concentration of phytoplankton pigments by measuring the radiance backscattered out of the water.[1–3] Only the first four bands (henceforth referred to as λ_1, λ_2, λ_3, and λ_4) had sufficient radiometric sensitivity to be useful for measuring the backscattered radiance. The next generation of ocean-color sensors, such as the Sea-Viewing-Wide-Field-of-View-Sensor[4] (SeaWiFS) and the Moderate-Resolution Imaging Spectroradiometer[5] (MODIS), will have a radiometric sensitivity superior to CZCS owing to an increased signal-to-noise ratio and a smaller quantization interval. They also will be equipped with additional spectral bands, e.g., a band near 412 nm to separate the detrital and viable phytoplankton signals, and bands centered on 765 and 865 nm to aid atmospheric correction. Our goal is to refine the CZCS atmospheric-correction algorithm[6–12] to utilize the new spectral bands and the increased sensitivity to improve the accuracy of the pigment retrieval. A by-product of this atmospheric-correction algorithm is an estimate of the aerosol optical thickness.

In earlier papers[13,14] we simulated the influence of wind-induced sea-surface roughness on the quality of the retrieval of the water-leaving radiances from an ocean-color sensor when a CZCS-type algorithm, which assumes a *flat* ocean, is used. We reached three significant conclusions for situations in which there is no direct sun glitter in the image (e.g., when there is either a large solar zenith angle or the sensor is tilted away from the specular image of the sun): First, the error induced by ignoring surface roughness is usually $\lesssim 1$ CZCS digital count for wind speeds up to ≈ 17 m/s, and therefore it can be ignored for that sensor. Next, the roughness-induced error is much more strongly dependent on the wind speed than on the shadowing of one wave by another, suggesting that surface effects can be adequately

The authors are with the Department of Physics, University of Miami, P.O. Box 248046, Coral Gables, Florida 33124-8046.

Received 1 February 1993; revised manuscript received 9 June 1993.

0003-6935/94/030443-10$06.00/0.

dealt with without a precise knowledge of wave shadowing. Finally, the error induced by ignoring multiple scattering is usually larger than that caused by ignoring surface roughness, suggesting that, in refining algorithms for future sensors, more effort should be placed on dealing with multiple scattering than on roughness of the sea surface. In the present paper, we present a preliminary algorithm for the atmospheric correction of the more sensitive SeaWiFS instrument.

We begin by reviewing the CZCS-correction algorithm and show that CZCS does not have a sufficient number of spectral bands to permit atmospheric correction on a pixel-by-pixel basis without the introduction of additional assumptions. Next, we examine the possibility of employing the additional spectral bands in the NIR to effect an atmospheric correction under the assumption of single scattering. Finally, we propose a scheme for dealing with multiple scattering, which leads to the preliminary algorithm.

CZCS Correction Algorithm

We begin with the definition of reflectance ρ:

$$\rho = \pi L / F_0 \cos \theta_0, \tag{1}$$

where L is the upward radiance in the given viewing direction, F_0 is the extraterrestrial solar irradiance, and θ_0 is the solar zenith angle. With this normalization for L, ρ determined at the top of the atmosphere would be the albedo of the ocean-atmosphere system if L were independent of the viewing angle. Because it is often more convenient to work with dimensionless reflectance (ρ) rather than radiance (L), and because the new sensors may be calibrated in reflectance instead of radiance, we shall abandon L in favor of ρ in this paper. Note, however, that given F_0, the transformation from one to the other is trivial. We can write the total reflectance, at a wavelength λ, measured at the top of the atmosphere as

$$\rho_t(\lambda) = \rho_r(\lambda) + \rho_a(\lambda) + \rho_{ra}(\lambda) + \rho_g(\lambda) + t\rho_w(\lambda), \tag{2}$$

where ρ_r is the reflectance resulting from multiple scattering by air molecules (Rayleigh scattering) in the absence of aerosols, ρ_a is the reflectance resulting from multiple scattering by aerosols in the absence of air, ρ_{ra} is the interaction term between molecular and aerosol scattering,[15] ρ_g is the reflectance of the direct solar beam, i.e., photons that are specularly reflected from the (rough) ocean surface, and ρ_w is the water-leaving reflectance. The ρ_g term in the above equation is generally ignored because ocean-color sensors are equipped with a provision for tilting the scan plane away from the specular image of the sun. It will also be ignored here. The term ρ_{ra} accounts for the interaction between Rayleigh and aerosol scattering, e.g., photons first scattered by the air then scattered by aerosols, or photons first scattered by aerosols then by the air. This term is zero in the single-scattering case, in which photons are only scattered once, and can be ignored as long as the amount of multiple scattering is small, i.e., at small Rayleigh and aerosol optical thicknesses.

The purpose of atmospheric correction is to retrieve ρ_w from the above equation. In principle the reflectances $\rho_r + \rho_a + \rho_{ra}$ could be removed if the concentration and optical properties of the aerosol were known throughout an image. The aerosol, however, is highly variable, and unlike the Rayleigh-scattering component ρ_r, the effects of $\rho_a + \rho_{ra}$ on the imagery cannot be predicted *a priori*. In the CZCS atmospheric-correction algorithm the term ρ_{ra} is ignored, and it is assumed that ρ_a can be replaced by its single-scattering value ρ_{as}.[7,8,10–12,16] Equation (2) then becomes

$$\rho_t(\lambda) = \rho_r(\lambda) + \rho_{as}(\lambda) + t\rho_w(\lambda), \tag{3}$$

where

$$\begin{aligned} \rho_{as}(\lambda) &= \omega_a(\lambda)\tau_a(\lambda)p_a(\theta, \theta_0, \lambda)/4 \cos\theta \cos\theta_0, \\ p_a(\theta, \theta_0, \lambda) &= P_a(\theta_-, \lambda) + [r(\theta) + r(\theta_0)]P_a(\theta_+, \lambda), \\ \cos\theta_\pm &= \pm \cos\theta_0 \cos\theta - \sin\theta_0 \sin\theta \cos(\phi - \phi_0), \end{aligned} \tag{4}$$

and $r(\theta)$ is the Fresnel reflectance of the interface for an incident angle θ. The parameters $\tau_a(\lambda)$, $\omega_a(\lambda)$, and $P_a(\alpha, \lambda)$ are, respectively, the aerosol optical thickness, the aerosol single-scattering albedo, and the aerosol scattering phase function for a scattering angle α. The angles θ_0 and ϕ_0 are the zenith and azimuth angles, respectively, of a vector from the point on the sea surface under examination (pixel) to the sun; likewise, θ and ϕ are the zenith and azimuth angles of a vector from the pixel to the sensor. In what follows we take $\phi_0 = 0$.

The general approach of the correction algorithm is to use spectral bands for which ρ_w is known to make an assessment of the aerosol contribution. For this, one band is required for assessing the magnitude of the aerosol's contribution, and a second is required for assessing its dependence on wavelength. Also, to extrapolate (or interpolate) the aerosol contribution to the other bands, a rule governing the spectral variation of ρ_{as} is required. For clear ocean water (phytoplankton-pigment concentration C less than 0.25 mg/m^3) ρ_w can be considered known[16] for CZCS bands 2, 3, and 4. Thus, in clear water there are enough spectral bands to estimate $\rho_w(\lambda_1)$, which is a very sensitive function of C and can be used to estimate the actual value of C. In the past, the error in the retrieved $\rho_w(\lambda_1)$ in clear water has been used in numerical simulations to study the efficacy of the correction algorithm and its assumptions.[11,14] It will be used in the same manner here.

The algorithm is operated by defining the atmospheric-correction parameters $\varepsilon(\lambda_i, \lambda_j)$:

$$\varepsilon(\lambda_i, \lambda_j) \equiv \frac{\rho_{as}(\lambda_i)}{\rho_{as}(\lambda_j)} = \frac{\omega_a(\lambda_i)\tau_a(\lambda_i)p_a(\theta, \theta_0, \lambda_i)}{\omega_a(\lambda_j)\tau_a(\lambda_j)p_a(\theta, \theta_0, \lambda_j)}. \tag{5}$$

Then, we compute $\varepsilon(\lambda_2, \lambda_4)$, $\varepsilon(\lambda_3, \lambda_4)$, and $\varepsilon(\lambda_4, \lambda_4)$ from

$\rho_{as}(\lambda_2)$, $\rho_{as}(\lambda_3)$, and ρ_{as} (λ_4), and extrapolate to find $\varepsilon(\lambda, \lambda_4)$ for any λ, e.g., λ_1, by assuming that

$$\varepsilon(\lambda, \lambda_4) = \left(\frac{\lambda_4}{\lambda}\right)^n. \quad (6)$$

Finally, $\rho_{as}(\lambda_1) = \varepsilon(\lambda_1, \lambda_4)\rho_{as}(\lambda_4)$, yielding $t(\lambda_1)\rho_w(\lambda_1)$ by means of Eq. (3). The diffuse transmittance t of the atmosphere is given approximately by[9]

$$t = \exp[-(\tau_r/2 + \tau_{Oz})/\cos\theta],$$

where τ_r is the Rayleigh optical thickness (molecular scattering) and τ_{Oz} is the ozone optical thickness. Note the requirement of at least two bands for which ρ_w is given (three are available in this example) so that ρ_{as} can be computed, and of the need for an extrapolation law, i.e., Eq. (6).

For pigment concentrations greater than 0.25 mg/m^3, ρ_w is no longer known for bands 2 and 3 so this procedure cannot be applied. One procedure that has been used is to first locate clear water in the image, then apply the above procedure, and finally use the resulting ε values for the entire image.[9] The drawbacks to this are the paucity of clear water in many images and the fact that the true ε may not be constant over the image. Bricaud and Morel[17] and André and Morel[18] have devised an alternate approach that uses a model-produced relationship between $\rho_w(\lambda_i)$ and C, *assumes* Eq. (6) is valid with an unknown n, and solves the resulting nonlinear equations at each pixel for C and n by iteration. However, the fact remains that, except in clear water, there is not sufficient information to perform atmospheric correction in the *general* case. In fact, thus far in the analysis of the CZCS global data set,[19] the values of ε have been set to unity (a very plausible value for marine aerosols) for all of the processing to effect a solution.

Application of the CZCS Algorithm to SeaWIFS

The next ocean-color sensor to fly in space is the Sea-viewing-Wide-Field-of-view-Sensor[4] (SeaWiFS). The radiometric specifications for SeaWiFS are presented in Table 1, in which ρ_{max} is the saturation reflectance, ρ_w is the water-leaving reflectance for clear ocean water, e.g., the Sargasso Sea, ρ_t is a typical value of the total radiance and $NE\Delta\rho$ is the noise equivalent reflectance. As ρ_w is essentially zero for SeaWiFS bands 7 and 8, it is logical to use these bands to assess the aerosol properties, i.e., to determine $\varepsilon(765,865) = \rho_{as}(765)/\rho_{as}(865)$ and use it to deduce $\varepsilon(\lambda, 865)$. However, noting that the total spectral region covered varies by over a factor of two in wavelength, it is not clear that the extrapolation provided by Eq. (6) will be valid.

Table 1. SeaWiFS Performance for $\theta_0 = 60°$ at the Scan Edge

Band	λ (nm)	ρ_{max}	ρ_w	ρ_t	$NE\Delta\rho$[a]
1	402–422	0.50	0.040	0.34	0.00068
2	433–453	0.46	0.038	0.29	0.00043
3	480–500	0.36	0.024	0.23	0.00034
4	500–520	0.30	0.0096	0.19	0.00031
5	545–565	0.25	0.0040	0.154	0.00027
6	660–680	0.17	0.0004	0.105	0.00023
7	745–785	0.15	—[b]	0.081	0.00018
8	845–885	0.13	—[b]	0.069	0.00015

[a]Noise equivalent reflectance.
[b]ρ_w < 1 digital count.

To try to gain some insight into the possible behavior of $\varepsilon(\lambda, 865)$, we have computed it for several aerosol models. The aerosol models we used were developed by Shettle and Fenn[20] for LOWTRAN-6.[21] In particular, we considered their maritime and tropospheric models and introduced a coastal model containing half the fraction of the sea salt aerosol that was in the maritime model. The coastal model simulates situations that may be expected to occur near the coast (i.e., with a larger continental influence). From the resulting size distributions and refractive indices, we used Mie theory to compute the aerosol optical properties for the SeaWiFS bands as a function of the relative humidity (RH). From these, $\varepsilon(\lambda, 865)$ is found. Sample results of this exercise are presented in Figs. 1(a) and 1(b). These computations suggest that there should be a strong variation of ε with aerosol model and RH. The increase in particle size (due to swelling) with increasing RH clearly reduces the spectral variation of ε. The spectral variation of ε owes in large part to the spectral variation of τ_a; however, additional variation is produced by the aerosol phase function, which was assumed to be independent of λ in the earlier CZCS algorithm.

Equation (6) suggests that there is a linear relationship between $\log(\varepsilon)$ and $\log(\lambda)$ of slope $-n$; however, Fig. 1(b), which provides the computations in Fig. 1(a) plotted in this format, shows that for most models this is a poor approximation for the variation of $\varepsilon(\lambda, 865)$ taken over the entire range of λ. Nevertheless, it is interesting to note that over the restricted range 443–670 nm, Eq. (6) is a reasonable approximation, and that using it to extrapolate ε from 520, 550, and 670 nm to 443 nm can be quite accurate. This may explain the success of such extrapolations with CZCS.

Continuing with the single-scattering approximation, we can estimate the error $\Delta\varepsilon$ that can be tolerated in ε for a given error in $t(\lambda)\Delta\rho_w(\lambda)$. This is

$$\Delta\varepsilon(\lambda, 865)\rho_{as}(865) = t(\lambda)\Delta\rho_w(\lambda).$$

A goal of SeaWiFS is to be able to recover ρ_w with an error of no more than 5%. For clear water ($C \lesssim 0.2$ mg/m^3) at 443 nm, $\rho_w \gtrsim 0.02$ which implies the error in $\rho(443)$, $\Delta\rho_w(443)$, should be $\lesssim 0.001$. Ignoring the factor t, which is between 0.8 and 0.9, we have

$$\Delta\varepsilon(443, 865) \approx \pm\frac{0.001}{\rho_{as}(865)}.$$

Because $\rho_{as} \propto \tau_a$, the required accuracy in $\varepsilon(443, 865)$ is increased as the turbidity of the atmosphere in-

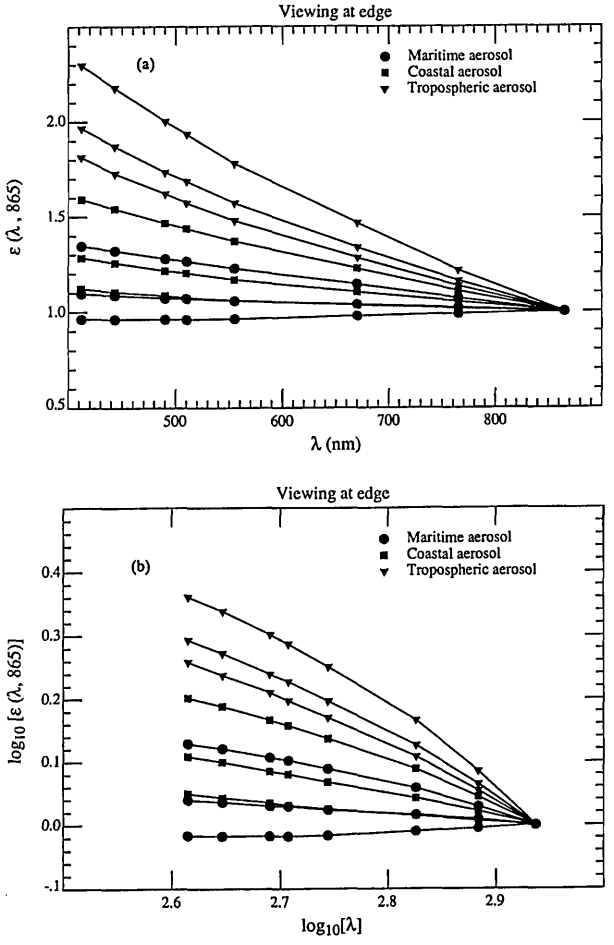

Fig. 1. $\varepsilon(\lambda, 865)$ as a function of λ for viewing at the edge and the center of the SeaWiFS scan with $\theta_0 = 60°$ for the maritime, coastal, and tropospheric aerosol models. For each model, the RH values are 70%, 90%, and 98% from the upper to the lower curves. (b) Same as (a) but plotted in log–log format.

creases. Reddy et al.[22] report a mean τ_a over the North Atlantic of ≈ 0.1 near 800 nm in situations where air-mass-trajectory analysis suggests the presence of only a maritime aerosol, and ≈ 0.2 when both continental and marine aerosols are expected to be present. Using the maritime or coastal models with RH = 90% to represent these two situations, the model predicts (for $\theta_0 = 60°$ at the scan edge) that $\rho_{as}(865) \approx 0.066\,\tau_a(865)$. Thus

$$\Delta\varepsilon(443, 865) \lesssim \pm \frac{0.015}{\tau_a(865)}$$

should lead to an error of less than 5% in $\rho_w(443)$ in clear water. This yields $\Delta\varepsilon \lesssim 0.15$ and 0.08 for $\tau_a = 0.1$ and 0.2, respectively. Thus, under average conditions in the North Atlantic, we must require $\Delta\varepsilon \lesssim \pm 0.10$ [or $\Delta \log \varepsilon \lesssim \pm 0.043/10^{\log \varepsilon}$ for Figure 1(b)] for $\theta_0 = 60°$ at the scan edge. Figure 1(b) shows that this limit is not met when ε is extrapolated according to Eq. (6) and RH < 90% for the maritime and coastal models, or for any of the tropospheric models. Figure 1(a) shows that a linear extrapolation ($\varepsilon \propto \lambda$) does not perform significantly better in this example.

Under extreme conditions, $\tau_a(865)$ can be significantly larger than 0.2 and still not saturate the sensor (see Table 5 below). In these cases the required $\Delta\varepsilon$ will be correspondingly smaller. We conclude then that to the extent that these aerosol models approximate reality, they suggest that a simple extrapolation of the derived value of $\varepsilon(765, 865)$, or even $\varepsilon(670, 765)$ or $\varepsilon(670, 865)$, to shorter wavelengths will be *difficult* and will limit the accuracy of the algorithm in this simplified (single-scattering) analysis.

A possible scheme for improving extrapolation is to base it on models [or on an experimental data base of $\varepsilon(765, 865)$ values]. For example, if the derived value of $\varepsilon(765, 865)$ falls midway between the values predicted by two models, we assume that $\varepsilon(\lambda, 865)$ will also fall midway between the two models for all λ. We have applied this idea to try to derive $\varepsilon(443, 865)$ from $\varepsilon(765, 865)$ for the maritime, coastal, and tropospheric aerosols at RH = 80%. For the cases examined below, i.e., $\theta_0 = 0°$, 20°, 40°, and 60°, at both the scan center and the scan edge, $\Delta\varepsilon(443, 865) < 0.02$ for all cases except one (where it was 0.0201), and was often < 0.01. Thus, this assumption that aerosols with similar $\varepsilon(765, 865)$ also have similar $\varepsilon(\lambda, 865)$ seems to be borne out by the aerosol models considered here; however, in the final analysis its validity must rest on experimental observations not now available. Given a well-calibrated SeaWiFS, it will be possible to test the hypothesis by studying $\varepsilon(\lambda, 865)$ for $\lambda \gtrsim 520$ nm over clear-water areas, for which $\rho_w(\lambda)$ is known.

Actually, we found that the variation of $\varepsilon(\lambda_i, \lambda_j)$ with wavelength over the entire-range of SeaWiFS bands could be represented well by a simple formula of the form $\varepsilon(\lambda_i, \lambda_j) = \exp[c(\lambda_j - \lambda_i)]$, where c depends on the viewing geometry and the aerosol model. Extrapolation of $\varepsilon(765, 865)$ obtained using this formula was as good as that obtained using the models. In fact, we have used this observation to modify the CZCS algorithm for use with SeaWiFS.[23] The modified CZCS algorithm works reasonably well when $\tau_a(865)$ is small, e.g., when $\tau_a(865) = 0.2$, we find $\Delta\rho_w \lesssim \pm 0.002$ for the maritime and the coastal models compared with the required ± 0.001. Unfortunately, it ignores multiple scattering, and the performance of the modified CZCS algorithm degrades rapidly as $\tau_a(865)$ increases, e.g., when $\tau_a(865) = 0.4$ with the tropospheric model at RH = 80%, $\Delta\rho_w(440) \lesssim -0.04$ at the edge of the SeaWiFS scan with $\theta_0 = 60°$ compared to -0.006 using an algorithm that includes multiple scattering as described below. Because the aerosol models seem to be required to address multiple scattering (discussed in the next section), we chose to use them to effect the ε extrapolation as well.

Multiple Scattering

Our analysis thus far has been based on the assumption of single scattering; however, multiple-scattering

effects have been shown[11,12,15] to be significant at the level of accuracy required for SeaWiFS, i.e., $\Delta\rho_w(443) \approx 0.001$. The single-scattering solution has been used to simplify the mathematics, to demonstrate the ε-extrapolation difficulty, and to suggest an approach for the correction. It has also been used in the spirit that, if the correction cannot be made—at least conceptually—at the required accuracy in a singly scattering atmosphere, it is hopeless in a multiply scattering regime.

When multiple scattering is included, atmospheric correction requires estimating the unknown $\rho_a(\lambda) + \rho_{ra}(\lambda)$ from its values at 765 and 865. These can be found because $\rho_w = 0$ at both wavelengths. Wang[24] has shown that a near-linear relationship exists between $\rho_a(\lambda) + \rho_{ra}(\lambda)$ and $\rho_{as}(\lambda)$. Examples of such a relationship are shown in Figs. 2(a) and 2(b) at 443 and 865 nm, respectively, for the tropospheric model with RH = 70% and the maritime model with RH = 98%. At a given value of τ_a, the increase in reflectance from 443 to 865 nm in these figures owes to the fact that P_a is larger in backscattering directions at 865 than at 443 nm. The single-scattering result (the 1:1 line), on which the preceding analysis was based, is also shown in the figures. The strong multiple scattering, even at 865 nm, means that it must be removed if one is to accurately estimate $\varepsilon(765, 865)$. We have experimented with several techniques for estimating $\varepsilon(765, 865)$. The best one we have found is to assume that the aerosol belongs to a given aerosol model, e.g., the ith model, for the given geometry and model; to solve the radiative transfer equation and derive the $\rho_a(\lambda) + \rho_{ra}(\lambda)$ versus $\rho_{as}(\lambda)$ relationships; to use these to estimate $\rho_{as}(765)$ and $\rho_{as}(865)$ to provide $\varepsilon_i(765, 865)$; and to average the ε's derived for a large number (N) of likely models, i.e.,

$$\varepsilon(765, 865) = \frac{1}{N}\sum_{i=1}^{N} \varepsilon_i(765, 865).$$

This works reasonably well because the values of ε derived using the individual models are all close to the correct value, i.e., for any given model the multiple-scattering effects are nearly the same at 765 and 865 nm. The weak Rayleigh-scattering contribution at these wavelengths results in a very small ρ_{ra}.

Having derived a value for $\varepsilon(765, 865)$, the next task is to estimate $\varepsilon(\lambda, 865)$. In general, the derived value of $\varepsilon(765, 865)$ will fall between those for two of the N aerosol models. We then assume that $\varepsilon(\lambda, 865)$ falls between the same two aerosol models proportionately in the same manner as $\varepsilon(765, 865)$, as suggested above. Note that $\varepsilon(\lambda, 865)$ relates $\rho_{as}(\lambda)$ to $\rho_{as}(865)$; however, rather than $\rho_{as}(\lambda)$, we desire $\rho_a(\lambda) + \rho_{ra}(\lambda)$. Thus we must make a transformation similar to that shown in Fig. 2(a). We effect this by using the two aerosol models that most closely bracketed $\varepsilon(765, 865)$, and assume that the $\rho_a(\lambda) + \rho_{ra}(\lambda)$ versus $\rho_{as}(\lambda)$ relationship falls between that for the two aerosol models in the same proportion as $\varepsilon(765, 865)$. The

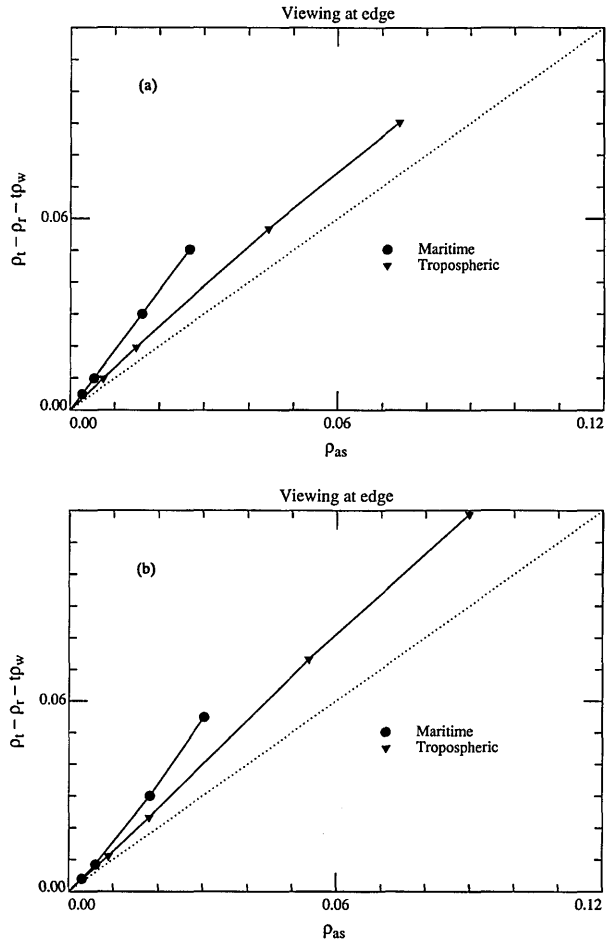

Fig. 2. $\rho_a(\lambda) + \rho_{ra}(\lambda)$ as a function of $\rho_{as}(\lambda)$ at the edge of the SeaWiFS. Upper solid curve is for the tropospheric model with RH = 70%; lower solid curve is for the maritime model with RH = 98%; and the dotted curve is the single-scattering result: (a) is for $\lambda = 443$ nm and $\theta_0 = 60°$; (b) is for $\lambda = 865$ nm and $\theta_0 = 60°$.

entire correction algorithm can be summarized schematically as follows:

$$t\rho_w(\lambda) = \rho_t(\lambda) - \rho_r(\lambda) - [\rho_a(\lambda) + \rho_{ra}(\lambda)],$$

$$\rho_t(765) - \rho_r(765) \text{ and } \rho_t(865) - \rho_r(865)$$

$$\xrightarrow{N \text{ Models}} \varepsilon(765, 865) \rightarrow 2 \text{ Models},$$

$$\varepsilon(765, 865) \xrightarrow{2 \text{ Models}} \varepsilon(\lambda, 865),$$

$$\rho_{as}(865) \xrightarrow{\varepsilon(\lambda, 865)} \rho_{as}(\lambda),$$

$$\rho_{as}(\lambda) \xrightarrow{2 \text{ Models}} \rho_a(\lambda) + \rho_{ra}(\lambda).$$

We note that the aerosol models used to address multiple scattering are those that most closely agree with the derived value of $\varepsilon(765, 865)$. This places a premium on accurately deriving this quantity.

To try to assess the efficacy of these ideas, we have

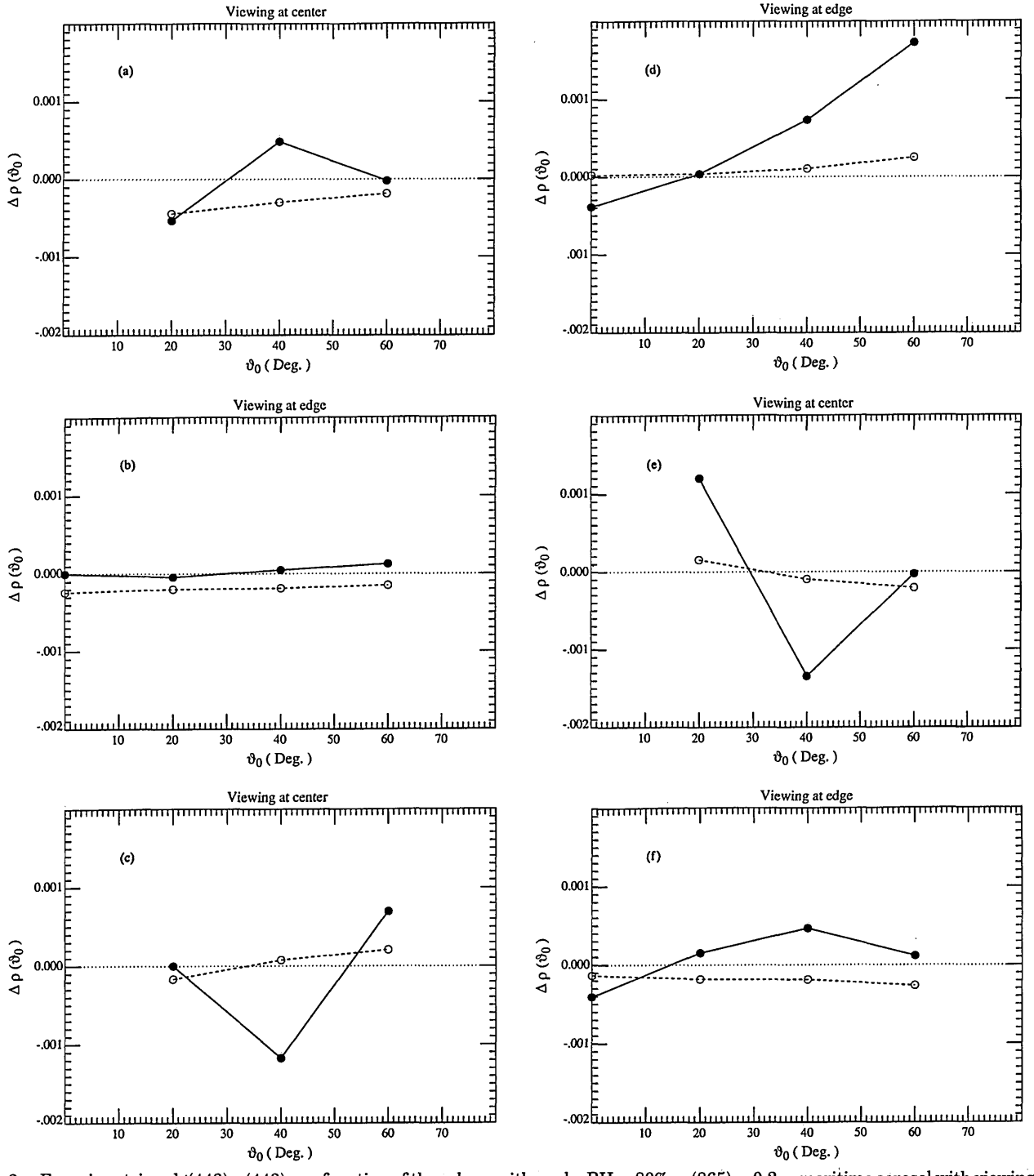

Fig. 3. Error in retrieved $t(443)\rho_w(443)$ as a function of the solar zenith angle; RH = 80%; $\tau_a(865) = 0.2$: maritime aerosol with viewing at (a) the center and (b) the edge of the scan; coastal aerosol with viewing at (c) the center and (d) the edge of the scan; and tropospheric aerosol with (e) the center and (f) the edge of the scan.

applied them to a series of simulations carried out using the models with RH = 80%, i.e., $\rho_t(\lambda)$ was simulated [with $\rho_w(\lambda) = 0$] for RH = 80%. These simulations were inserted into the above algorithm with the maritime, coastal, and tropospheric models for RH = 70%, 90%, and 98% serving as the $N = 9$ candidate aerosol models. The error in the recovered water-leaving reflectance, $\Delta\rho(\lambda) \equiv t(\lambda)\Delta\rho_w(\lambda)$, was computed. Note that the aerosol models used in the simulations were similar, but not identical, to all of the nine candidate models. The simulations were carried out for $\theta_0 = 0$, 20°, 40°, and 60°, the viewing was assumed to be at the center (nadir) and the edge (viewing angle $\approx$ 45°, ϕ = 90°) of the scan. $\tau_a(865)$ was taken to be 0.2, which is approximately 2 to 3 times the average for the North Atlantic with a pure

maritime atmosphere.[22] The results are shown in Figs. 3(a)–3(f) (solid curves). There is no value plotted at the scan center for $\theta_0 = 0$ because, in that viewing geometry, ρ_t would be strongly contaminated by sun glitter. The results suggest that the proposed algorithm is close to producing the ± 0.001 accuracy in the water-leaving reflectance at 443 nm under most circumstances.

Figures 3(a)–3(f) (dashed curves) also include the error in $t\rho_w$ that the algorithm would have if the correct physics of the atmosphere were single scattering, i.e., if the dotted curves in Figs. 2(a) and 2(b) were applicable. In this case, $\varepsilon(765, 865)$ is determined exactly, so the error owes entirely to the extrapolation from $\varepsilon(765, 865)$ to $\varepsilon(443, 865)$. Clearly, $t\Delta\rho_w$ is usually larger when there is significant multiple scattering; however, the results suggest that complications arising from multiple scattering are addressed rather well with the present algorithm.

We have examined other aerosol models that differ considerably from those of Shettle and Fenn,[20] e.g., Jung[25] power-law distributions with all of the particles characterized by a single, wavelength-independent refractive index. We find that in the case of aerosols for which the size-refractive index distribution is broadly similar to one of the nine candidate models used here, the error is sufficiently small that it can be plotted on the same scale as Fig. 3 when $\tau_a(865) = 0.2$. In contrast, when models are used that are not similar to one of our nine basic models, e.g., a model that resembles the tropospheric aerosol at RH = 70% but with no aerosol absorption, very large errors can occur ($|\Delta\rho| > 0.01$). Thus it is imperative that the size-refractive index distribution of the N candidate models encompass the actual range of parameters for natural aerosols over the ocean.

To see the influence of the aerosol concentration, we have also carried out simulations with $\tau_a(865) = 0.4$—a turbid atmosphere over the oceans.[15] Samples of the results for the maritime aerosol are presented in Fig. 4, in which $\Delta\rho$ is compared for $\tau_a(865) = 0.2$ and 0.4. One sees that the algorithm performs nearly as well for the more turbid atmosphere. Figure 4 also includes the results of simulations carried out for a wind-roughened surface.[13,14] In this case, the wind speed W was 7.5 m/s; however, it was assumed to be zero in the computation of ρ_r, and the algorithm operated as described above. In the cases presented, only a modest gain in accuracy would be achieved by knowing the wind speed.

Finally, we estimate the effect that these errors in the atmospheric correction have on the accuracy of the retrieved pigment concentration. The blue–green radiance ratio given by the semianalytic model of Gordon et al.[26] can be represented well by the expression

$$\log_{10} 3.33C = -1.2 \log_{10} r_L + 0.5(\log_{10} r_L)^2 - 2.8(\log_{10} r_L)^3, \quad (7)$$

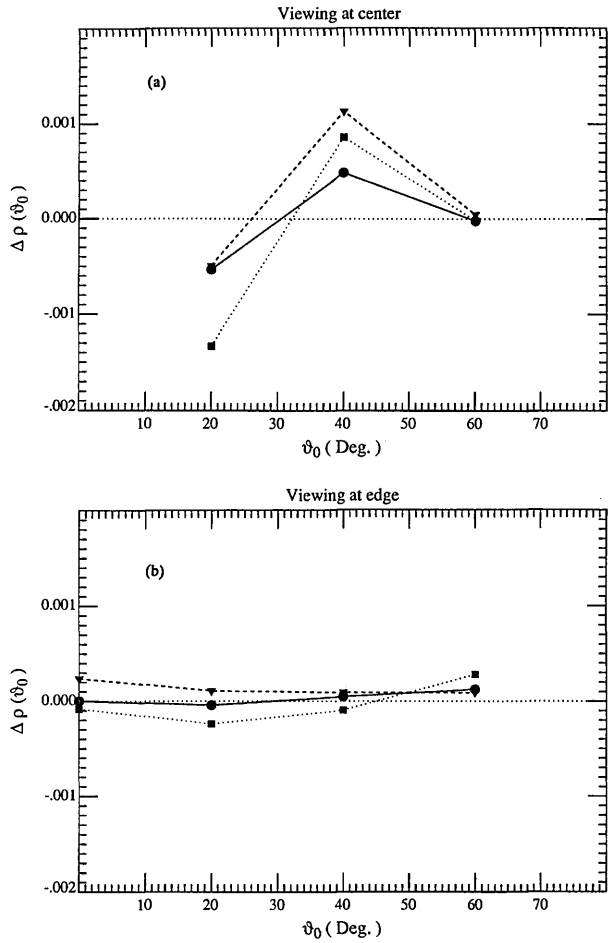

Fig. 4. Examples of the performance of the proposed algorithm at (a) the scan center and (b) the scan edge for a maritime aerosol when $\tau_a(865)$ is increased from 0.2 (circles) to 0.4 (squares), and when $\tau_a(865) = 0.2$ but the surface is roughened by a 7.5 m/s wind (triangles), which is ignored in the operation of the algorithm.

where

$$r_L = \frac{1}{2}\frac{[L_w(443)]_N}{[L_w(550)]_N},$$

and $[L_w(\lambda)]_N$ is the normalized water-leaving radiance[16] at λ, i.e.,

$$tL_w(\lambda) = [L_w(\lambda)]_N \cos\theta_0 \times \exp\left[-\left(\frac{\tau_r}{2} + \tau_{Oz}\right)\left(\frac{1}{\cos\theta_0} + \frac{1}{\cos\theta}\right)\right].$$

Approximate values of $[L_w(\lambda)]_N$ for two values of C are given in Table 2. From $\Delta\rho = t\Delta\rho_w$ in Figs. 3(a)–3(f), and similar computations at 555 nm, where $t\Delta\rho_w$ is approximately half of that at 443 nm, it is possible to compute the actual values of $[L_w(\lambda)]_N$ that would be retrieved by the atmospheric-correction algorithm. Inserting these into Eq. (7), and neglecting the difference between $\lambda = 550$ nm (used by CZCS) and $\lambda = 555$ nm (to be used in SeaWiFS), the result for the pigment concentration is C'. The error in the re-

Table 2. $[L_w(\sqsubseteq)]_N$ for Two Pigment Concentrations

	$[L_w(\lambda)]_N$[b]	
C[a]	(λ = 443)	(λ = 550)
0.10	1.65	0.37
0.91	0.34	0.34

[a]C is the phytoplankton-pigment concentration (in mg/m^3).
[b]$[L_w(\lambda)]_N$ is the normalized water-leaving radiance in (mW/cm^2 μm Sr).

trieved pigment concentration, i.e., $\Delta C = C' - C$, is then determined. It was found that of the 42 simulations, ~95% had $\Delta C/C < \pm 30\%$, ~88% and $\Delta C/C < \pm 20\%$, and ~69% had $\Delta C/C < \pm 10\%$. All of the cases with $\Delta C/C > \pm 20\%$ were for $C = 0.91$ mg/m^3, where the water-leaving reflectance is very small (~0.004) at both wavelengths.

Retrieval of τ_a

There is considerable interest now in the global distribution of aerosols because of their role in climate forcing and biogeochemical cycling.[27] The hypothesis[28] that dimethylsulfide (DMS) from phytoplankton activity leads to an increase in cloud condensation nuclei in the marine atmosphere argues for simultaneous study of aerosols and productivity where possible.[29] There has been effort in recent years directed toward estimating the aerosol concentration ($\propto \tau_a$) and other properties using Earth-orbiting satellites.[30–39] In this section we show that τ_a can be retrieved with a simple extension of the atmospheric-correction algorithm.

Even in the single-scattering approximation, one notes from Eq. (4) that it is not possible to estimate τ_a without assuming a model for the aerosol to provide ω_a and P_a. For example, Rao et al.[39] assume that the aerosol consists of spherical particles with a size–frequency distribution $\propto$ (radius)$^{-4.5}$ and a refractive index of 1.5. The assumption of an incorrect model can produce significant errors (up to factors of 2 to 3) in the recovered τ_a. As in atmospheric correction with SeaWiFS, we will try to avoid using an incorrect model in the retrieval of τ_a by using the only other aerosol information available on a pixel-by-pixel basis—the spectral variation of ρ_{as}.

Table 3. Error in Retrieved $\tau_a(865)$[a]

		Error (%) in $\tau_a(865)$		
Position	θ_0	Maritime	Coastal	Tropospheric
Center	20°	+10.9	−4.74	+2.02
	40°	−2.96	−5.04	+0.62
	60°	−0.31	−4.57	+0.94
Edge	0°	−1.36	−2.69	+0.43
	20°	−1.39	−3.73	+0.13
	40°	−1.75	−5.45	−0.29
	60°	−0.92	−5.74	+0.65

[a]Viewing at center and edge of the scan. The true value of $\tau_a(865)$ is 0.20.

Table 4. Error in Retrieved $\tau_a(865)$[a]

		Error (%) in $\tau_a(865)$		
Position	θ_0	Maritime	Coastal	Tropospheric
Center	20°	+9.99	−6.40	+1.01
	40°	−1.82	−6.36	+1.00
	60°	+0.83	−3.63	+1.32
Edge	0°	−0.52	−2.45	+0.99
	20°	−0.24	−2.99	+0.93
	40°	+0.03	−3.77	+0.90
	60°	+0.85	−3.95	+1.37

[a]Viewing at center and edge of the scan. The true value of $\tau_a(865)$ is 0.40.

Our retrieval algorithm is a simple extension of the atmospheric-correction algorithm, i.e., the correction algorithm yields the two models that most closely bracket $\varepsilon(765, 865)$, and we use these two models to invert Eq. (4) to obtain two estimates of τ_a. Using the same simulation set we used above to test the correction algorithm, we now examine the accuracy with which τ_a can be estimated. Briefly, we assume that the aerosol consists of particles that are accurately described by the maritime, coastal, or tropospheric aerosol models with RH = 80%. ρ_t is simulated for this aerosol and inserted into the atmospheric-correction algorithm. The correction algorithm provides two candidate models based on $\varepsilon(765, 865)$, and these specify two sets of P_a and ω_a values for two estimates τ_a. These estimates are then averaged to yield the final estimate of τ_a. Tables 3 and 4 provide the percent error in the retrieved $\tau_a(865)$ for three aerosol models at the center and the edge of the SeaWiFS scan as a function of θ_0. The true value of $\tau_a(865)$ was 0.2 or 0.4. All the calculations were carried out for $\phi = 90°$. From the tables, we can see that the error in the retrieved aerosol optical thickness is within ±10% (and usually considerably less) for most of the cases examined. We also tried determining τ_a from the weighted average of the two estimates as in the correction algorithm; however, this led to a slightly poorer estimate of retrieval.

Finally, it is of interest to estimate the upper limit to the value of $\tau_a(865)$ that can be estimated with SeaWiFS given its design saturation reflectance (ρ_{max}).

Table 5. Value of $\tau_a(865)$ Required for Saturation of SeaWIFS at 865 nm

		Maximum Value of $\tau_a(865)$	
Position	θ_0	Maritime[a]	Tropospheric[b]
Center	20°	0.72	0.54
	40°	1.04	0.72
	60°	1.69	0.80
Edge	0°	0.88	0.51
	20°	0.98	0.51
	40°	1.04	0.50
	60°	1.02	0.50

[a]RH = 98%.
[b]RH = 70%.

This is dependent on the particular aerosol model because, for a given τ_a, the backscattering (scattering at angles $> 90°$) is strongly dependent on the aerosol-size distribution and the refractive index. We estimate the upper limit of $\tau_a(865)$ that can be estimated by using the tropospheric model with RH = 70% (the largest backscattering of the models used here) and the maritime model with RH = 98% (the smallest backscattering). The results are presented in Table 5.

Concluding Remarks

In this paper we have presented an algorithm for atmospheric correction of second-generation ocean-color scanners with emphasis on SeaWiFS. Two concerns arise in applying the older CZCS algorithm to the more sensitive SeaWiFS: first, there is the extrapolation of the spectral variation of the aerosol reflectance from the NIR into the visible; and second, there is the influence of multiple scattering. Realistic aerosol models suggest that the previously used power-law-reflectance extrapolation is not likely to be valid (Fig. 1) because, although Eq. (6) applies rather well for the CZCS spectral range (443–670 nm), it is sometimes a very poor approximation for the SeaWiFS range [Fig. 1(b)]. The models also suggest that the effects of multiple scattering depend significantly on the particular aerosol model (Fig. 2), i.e., on the aerosol-scattering phase function. Thus it is necessary to have some information regarding the aerosol if one is to account correctly for multiple scattering. Guided by the models that we used here, we developed a systematic approach to carrying out the atmospheric correction. The basic hypothesis is that if $\varepsilon(765, 865)$ falls between two aerosol models, the reflectance $\rho_a + \rho_{ra}$ will fall between the same two models in the same proportion as $\varepsilon(765, 865)$. This is certainly not true in general; however, for the range of models that we have examined here, it appears to be accurate enough to effect correction to the desired accuracy, even in relatively turbid atmospheres. A simple extension of the algorithm provides an estimate of τ_a with an error of $\pm \lesssim 10\%$.

Our approach to the implementation of these ideas is to create a set of look-up tables in which $\rho_t - \rho_r - t\rho_w$ is provided as a function of ρ_{as} (Fig. 2). These tables will consist of several aerosol models that must encompass the expected natural range of the size-refractive index distribution, aerosol optical thicknesses, and all possible combinations of solar and viewing geometries. Operation of the algorithm will be similar to that presented above, with adaptation to the particular geometry made by interpolation. Because application of this new algorithm requires derivation of an accurate value for $\varepsilon(765, 865)$, high radiometric calibration is a necessity, as is removal of any component of ρ_t that is due to whitecaps[40,41] on the sea surface. Also, the 765-nm band overlaps the O_2 absorption band at 759 nm, so its influence on $\rho_t(765)$ needs to be assessed. We view all three of these requirements as major challenges; however, the O_2-absorption problem can be circumvented by utilizing the 670-nm band in place of the 765-nm band, at the expense of having to assess $\rho_w(670)$ in waters with $C \gtrsim 1\ \mathrm{mg/m^3}$.

We are not really comfortable with an atmospheric-correction algorithm that makes such extensive use of aerosol models. The difficulty with the models is twofold: First, although they were developed on the basis of measurements of the size distribution and index of refraction of aerosol particles, they obviously are simplifications of the actual physical and chemical properties of the aerosol. Second, their optical properties have been computed using Mie theory, i.e., assuming homogeneous, spherical particles. Such a simplification may yield realistic scattering and extinction coefficients, but could result in significant errors in the computed phase function,[42] particularly in the important backscattering directions. Our hope is that they provide a realistic approximation for $\varepsilon(\lambda_i, \lambda_j)$ and the multiple-scattering effects. However, at this point we see no more rational approach for achieving the required accuracy, considering that the effects of multiple scattering are model dependent. In the final analysis, their efficacy must be judged on the quality of the atmospheric correction that they produce.

Finally, we should remark that the proposed correction algorithm could also be based on measured, column-averaged, optical properties of the aerosol, e.g., those obtained by inverting at-sea sky-radiance and sun photometer measurements[43] to obtain $\tau_a(\lambda)$, $\omega_a(\lambda)$, and $P_a(\alpha, \lambda)$—the optical properties that the models provide. A comprehensive data base of such properties would circumvent the reliance on aerosol models and place the correction algorithm on a firmer foundation.

This work was supported by grant NAGW–273 and contracts NAS5–31363 and NAS5–31743 from the National Aeronautics and Space Administration.

References

1. W. A. Hovis, D. K. Clark, F. Anderson, R. W. Austin, W. H. Wilson, E. T. Baker, D. Ball, H. R. Gordon, J. L. Mueller, S. Y. E. Sayed, B. Strum, R. C. Wrigley, and C. S. Yentsch, "Nimbus 7 Coastal Zone Color Scanner: system description and initial imagery," Science **210,** 60–63 (1980).
2. H. R. Gordon, D. K. Clark, J. L. Mueller, and W. A. Hovis, "Phytoplankton pigments derived from the Nimbus–7 CZCS: initial comparisons with surface measurements," Science **210,** 63–66 (1980).
3. H. R. Gordon and A. Y. Morel, *Remote Assessment of Ocean Color for Interpretation of Satellite Visible Imagery: A Review* (Springer-Verlag, New York, 1983).
4. S. B. Hooker, W. E. Esaias, G. C. Feldman, W. W. Gregg, and C. R. McClain, *SeaWiFS Technical Report Series: Volume 1, An Overview of SeaWiFS and Ocean Color,* NASA Tech. Memo. 104566 (NASA Greenbelt Space Flight Center, Greenbelt, Md., July 1992).
5. V. V. Salomonson, W. L. Barnes, P. W. Maymon, H. E. Montgomery, and H. Ostrow, "MODIS: advanced facility instrument for studies of the earth as a system," IEEE Trans. Geosci. Remote Sensing **27,** 145–152 (1989).
6. H. R. Gordon, "Radiative transfer: A technique for simulat-

ing the ocean in satellite remote-sensing calculations," Appl. Opt. **15,** 1974–1979 (1976).
7. H. R. Gordon, "Removal of atmospheric effects from satellite imagery of the oceans," Appl. Opt. **17,** 1631–1636 (1978).
8. H. R. Gordon and D. K. Clark, "Atmospheric effects in the remote sensing of phytoplankton pigments," Boundary-Layer Meteorol. **18,** 299–313 (1980).
9. H. R. Gordon, D. K. Clark, J. W. Brown, O. B. Brown, R. H. Evans, and W. W. Broenkow, "Phytoplankton pigment concentrations in the Middle Atlantic Bight: comparison between ship determinations and Coastal Zone Color Scanner estimates," Appl. Opt. **22,** 20–36 (1983).
10. M. Viollier, D. Tanre, and P. Y. Deschamps, "An algorithm for remote sensing of water color from space," Boundary-Layer Meteorol. **18,** 247–267 (1980).
11. H. R. Gordon and D. J. Castaño, "The Coastal Zone Color Scanner atmospheric correction algorithm: multiple scattering effects," Appl. Opt. **26,** 2111–2122 (1987).
12. H. R. Gordon, J. W. Brown, and R. H. Evans, "Exact Rayleigh scattering calculations for use with the Nimbus 7 Coastal Zone Color Scanner," Appl. Opt. **27,** 862–871 (1988).
13. H. R. Gordon and M. Wang, "Surface roughness considerations for atmospheric correction of ocean color sensors. 1: Rayleigh scattering component," Appl. Opt. **31,** 4247–4260 (1992).
14. H. R. Gordon and M. Wang, "Surface-roughness considerations for atmospheric correction of ocean color sensors. 2: Error in the retrieved water-leaving radiance," Appl. Opt. **31,** 4261–4267 (1992).
15. P. Y. Deschamps, M. Herman, and D. Tanre, "Modeling of the atmospheric effects and its application to the remote sensing of ocean color," Appl. Opt. **22,** 3751–3758 (1983).
16. H. R. Gordon and D. K. Clark, "Clear water radiances for atmospheric correction of Coastal Zone Color Scanner imagery," Appl. Opt. **20,** 4175–4180 (1981).
17. A. Bricaud and A. Morel, "Atmospheric corrections and interpretation of marine radiances in CZCS imagery: use of a reflectance model," Oceanologica Acta **7,** 33–50 (1987).
18. J.-M. André and A. Morel, "Atmospheric corrections and interpretation of marine radiances in CZCS imagery, revisited," Oceanologica Acta **14,** 3–22 (1991).
19. G. C. Feldman, N. Kuring, C. Ng, W. Esaias, C. R. McClain, J. Elrod, N. Maynard, D. Endres, R. Evans, J. Brown, S. Walsh, M. Carle, and G. Podesta, "Ocean color: availability of the global data set," EOS Trans. Am. Geophys. Union **70,** 634–641 (1989).
20. E. P. Shettle and R. W. Fenn, *Models for the Aerosols of the Lower Atmosphere and the Effects of Humidity Variations on Their Optical Properties,* Rep. AFGL-TR-79-0214, (U.S. Air Force Geophysics Laboratory, Hanscom Air Force Base, Mass., 1979).
21. F. X. Kenizys, E. P. Shettle, W. O. Gallery, J. H. Chetwynd, L. W. Abreu, J. E. A. Selby, S. A. Clough, and R. W. Fenn, *Atmospheric Transmittance/Radiance: The LOWTRAN 6 Model,* Rep. AFGL-TR-83-0187, NTIS AD A 137796 (U.S. Air Force Geophysics Laboratory, Hanscom Air Force Base, Mass., 1983).
22. P. J. Reddy, F. W. Kreiner, J. J. Deluisi, and Y. Kim, "Aerosol optical depths over the Atlantic derived from shipboard sunphotometer observations during the 1988 Global Change Expedition," Global Biogeochemic. Cycles **4,** 225–240 (1990).
23. M. Wang and H. R. Gordon, "Remote sensing of environment," a simple, moderately accurate, atmospheric correction algorithm for SeaWiFS, (submitted to Remote Sensing Environ.).
24. M. Wang, "Atmospheric correction of the second generation ocean color sensors," Ph.D. dissertation (University of Miami, Coral Gables, Fla., 1991).
25. C. Junge, "Atmospheric chemistry," Adv. Geophys. **4,** 1–108 (1958).
26. H. R. Gordon, O. B. Brown, R. H. Evans, J. W. Brown, R. C. Smith, K. S. Baker, and D. K. Clark, "A semi-analytic radiance model of ocean color," J. Geophys. Res. **93D,** 10909–10924 (1988).
27. R. J. Charlson, S. E. Schwartz, J. M. Hales, R. D. Cess, J. A. Coakley, J. E. Hansen, and D. J. Hofmann, "Climate forcing by anthropogenic aerosols," Science **255,** 423–430 (1992).
28. R. J. Charlson, J. E. Lovelock, M. O. Andreae, and S. G. Warren, "Oceanic phytoplankton, atmospheric sulphur, cloud albedo, and climate," Nature (London) **326,** 655–661 (1987).
29. P. G. Falkowski, Y. Kim, Z. Kolber, C. Wilson, C. Wirick, and R. Cess, "Natural versus anthropogenic factors affecting low-level cloud albedo over the North Atlantic," Science **256,** 1311–1313 (1992).
30. M. Griggs, "Measurements of the aerosol optical thickness over water using ERTS-1 data," J. Air Pollut. Control Assoc. **25,** 622–626 (1975).
31. Y. Mekler, H. Quenzel, G. Ohring, and I. Marcus, "Relative atmospheric aerosol content from ERTS observations," J. Geophys. Res. **82,** 967–970 (1977).
32. M. Griggs, *AVHRR Measurements of Atmospheric Aerosols Over Oceans,* NOAA Final Rep. contract M0–A01–78–00–4092 (National Oceanic and Atmospheric Administration, National Environmental Satellite Service, Washington, D.C., November 1981).
33. M. Griggs, *Satellite Measurements of Tropospheric Aerosols,* NASA Contractor Rep. 3459 (NASA Langley Research Center, Hampton, Va., August 1981).
34. M. Griggs, AVHRR Aerosol Ground Truth Experiment, Final Rep. contract NA–83–SAC–00106 (National Oceanic and Atmospheric Administration, National Environmental Satellite Service, Washington, D.C., January 1984).
35. R. S. Fraser, "Satellite measurement of mass of Sahara dust in the atmosphere," Appl. Opt. **15,** 2471–2479 (1976).
36. P. Koepke and H. Quenzel, "Turbidity of the atmosphere determined from satellite: calculation of optimum viewing geometry," J. Geophys. Res. **84,** 7847–7856 (1979).
37. P. Koepke and H. Quenzel, "Turbidity of the atmosphere determined from satellite: calculation of optimum wavelength," J. Geophys. Res. **86,** 9801–9805 (1981).
38. P. A. Durkee, D. R. Jensen, E. E. Hindman, and T. H. V. Haar, "The relationship between marine aerosol particles and satellite-detected radiance," J. Geophys. Res. **91D,** 4063–4072 (1986).
39. C. R. N. Rao, L. L. Stowe, E. P. McClain, and J. Sapper, "Development and application of aerosol remote sensing with AVHRR data from the NOAA satellites," in *Aerosols and Climate,* P. Hobbs and M. P. McCormick, eds. (Deepak, Hampton, Va., 1988) pp. 69–80.
40. P. Koepke, "Effective reflectance of ocean whitecaps," Appl. Opt. **23,** 1816–1824 (1984).
41. E. C. Monahan and I. G. O'Muircheartaigh, "Whitecaps and the passive remote sensing of the ocean surface," Int. J. Remote Sensing **7,** 627–642 (1986).
42. A. Mugnai and W. J. Wiscombe, "Scattering from nonspherical Chebyshev particles. 3: Variability in angular scattering patterns," Appl. Opt. **28,** 3061–3073 (1989).
43. M. Wang and H. R. Gordon, "Retrieval of the columnar aerosol phase function and single-scattering albedo from sky radiance over the ocean: simulations," Appl. Opt. **32,** 4598–4609 (1993).